A multispectral Bayesian method for improved discrimination performance of seabed sediment classification using multi-frequency multibeam backscatter data

T. C. Gaida[1], T. A. Tengku Ali[1,3], M. Snellen[1,2], D. G. Simons [1]

1 Acoustics Group, Faculty of Aerospace Engineering, Delft University of Technology
2 Department of Applied Geology and Geophysics, Deltares
3 Department of Survey Science and Geomatics, Universiti Teknologi MARA, Perlis, Malaysia

Abstract

Seabed backscatter data collected from multibeam echosounders (MBES) can provide valuable information about various sediments types and habitats. The interest of employing different acoustic frequencies with the aim of increasing the discrimination performance between different sediment types becomes increasingly popular. Although several experimental studies have already shown and proven the strong dependency of acoustic backscatter strength on frequency. The field of satellite remote sensing has indicated the enormous potential of using multispectral data for several decades. However, just recently the R2Sonic 2026 MBES was introduced which allows to emit a series of signals over frequencies from 100 kHz to 400 kHz on a ping-by-ping basis. This study presents the working steps taken to process multispectral backscatter data. Followed by introducing an extension of the Bayesian method for seabed classification to multispectral backscatter including the application to a dataset acquired in the Bedford Basin, Canada in 2016. It is shown that this data can be properly processed to be used for acoustic seabed classification. The Bayesian method is successfully extended to multispectral backscatter data producing a so-called multispectral acoustic classification map while accounting for the probability of misclassification at a single frequency. The results of the Bayesian method indicate that sensing this study area with a frequency of 200 kHz and 400 kHz yields to the highest number of acoustic classes. There is, indeed, an increase in discrimination performance by using different frequencies. The combination of the most separated frequencies (100 kHz and 400 kHz) achieves the highest discrimination performance in this study area. These results indicate the potential for solving existing ambiguities in the relationship between single-frequency backscatter and certain sediment types. A correlation of the acoustic classes can only be found with soft, mixed and had substrata. The benefit of using several frequencies cannot clearly quantitatively assessed on the basis of the existing video footage. Still, a qualitative comparison indicates a correlation of more than three seabed types to the acoustic classes and, in addition, an improved discrimination between different sediment types by combining 100 kHz, 200 kHz and 400 kHz to a multispectral acoustic classification map.

1. Introduction

Multi-beam echo-sounders (MBES) have become the most valuable tool for ocean, geological and benthic habitat mapping for many years providing high-resolution sediment maps [1]. Various different classification strategies and methods employing MBES bathymetry, backscatter and their second order derivatives have been developed to characterize the seabed or riverbeds in the last two decades [2], thereby aiming to maximize the performance in discriminating between different sediment types or seabed features. Acoustic backscatter strength is the most common feature used in seabed classification [2]. The backscatter strength is related to seabed properties, such as sediment bulk density, seafloor roughness, volume heterogeneity, discrete scatterers and sediment layering [3], [4]. The influence of these factors on the backscatter strength is dependent on the composition of the seabed, angle of incidence and acoustic frequency [4]. Hence, by considering a constant incident angle, the interaction between the acoustic signal and the seabed depends solely on the frequency of the transmitted signal. In general, the frequency dependency of the backscatter strength is caused by three main factors: i) relationship between seabed roughness and acoustic wavelength [5], ii) dominating scattering regime, i.e. Rayleigh or geometrical scattering, which is influenced by the relationship between acoustic wavelength and particle size [6], [7], and iii) contribution of volume scattering influenced by signal penetration [4]. In several lab or field experiments, in which the influence of varying frequencies on the backscatter strength was studied, it was shown that specific sediment types have different acoustic responses for different frequencies [8], [3], [9]. The first acquisition and analysis of multispectral backscatter acquired with a co-located MBES operating at 70-100 kHz and 200-400 kHz was carried out by Hughes-Clark [10]. The study has shown a clear variation in the angular response curve shapes and differences in relative backscatter between the frequencies. These results provide promising opportunities to increase the discrimination performance of seabed sediments by utilizing different frequencies. However, MBES backscatter data is typically collected at one specific frequency or in a narrow band around the central frequency. R2Sonic has developed a broadband MBES (R2Sonic 2026), allowing to collect multispectral backscatter data using a single system. This MBES emits a series of signals at 100 kHz, 200 kHz and 400 kHz. In Brown *et al.* [11], the first multispectral backscatter dataset acquired with a single MBES system (R2Sonic 2026) in the Bedford Basin, Canada was employed. They introduced a false-color composite image obtained from the three single-

frequency backscatter mosaics as a visualization tool for multispectral backscatter.

However, the interest of employing different acoustic frequencies with the aim of increasing discrimination performance between sediment types is just at the beginning. The use of multispectral MBES data for seabed classification demands an appropriate data processing to account for the frequency dependency of environmental and sonar specific variables influencing the actual backscatter strength. Secondly, an appropriate classification technique has to be developed and applied to multispectral MBES backscatter data. In terrestrial remote sensing, the use of multispectral data and their classification has already been carried out and proven well for a long time. Acquiring data across a wide spectrum of electromagnetic wavelengths has increased the discrimination power of classification routines [12]. These benefits of using multiple frequencies were not available for the marine acoustic remote sensing community due to the lack of multi-frequency MBES's and appropriate classification methods in the last years.

In this study, the Bayesian method for seabed classification, which has already been successfully employed in previous studies to single frequency MBES datasets (e.g., [13], [14]), is applied to multispectral MBES backscatter data. The method accounts for the natural variability of the backscatter strength by assuming that the measured backscatter per beam resulting from a number of discrete seabed types corresponds to a sum of Gaussian distributions, where each Gaussian corresponds to a distinct seabed type [15]. The technique considers the backscatter strength per beam (or incident angle) separately. That means, by considering a constant incident angle, the backscatter strength is only dependent on frequency and seabed properties. In addition, the classification is independent on beam dependent sonar artefacts and is able to resolve across-track seafloor type changes on a beam footprint scale. One of the most important features of the Bayesian method is the statistical calculation of the optimal number of acoustic classes (AC), thus offering objective results.

As a first goal, this work aims to process the multispectral MBES dataset (100, 200 and 400 kHz) acquired in the Bedford Basin, Canada, with a particular focus on the frequency dependent environmental and sonar specific variables, to provide relative backscatter strength per frequency. Secondly, the study aims to develop a suitable classification method for multispectral MBES data. For the current research, the Bayesian method for seabed classification is extended to be applicable for multispectral backscatter. Finally, an evaluation and quantification of the

benefits of using several frequencies for acoustic seabed classification are carried out.

This paper is organized as follows. Section 2 provides an overview over the theoretical background of acoustic backscatter processing and the classification method used in this contribution. Section 3 gives an explanation of the study area and the multispectral MBES dataset. Section 4 presents the results of the acoustic data processing and the classification of multispectral data. In section 5 the results are discussed. Finally, the conclusions are drawn in section 6.

2. Theory

2.1. Acoustic data processing

Backscatter values can provide an indication of the nature and physical character of the seafloor. However, before any useful information can be extracted, it is necessary that the received acoustic signal is processed appropriately to retrieve actual backscatter strength *BS*. All terms affecting the backscatter strength are expressed by the sonar equation (modified from [16])

$$BS = EL - SL - G_r - Fr + 2TL - 10\log(A) \quad (1)$$

where *EL* is the intensity of the received echo which depends on the characteristics of the sonar such as source level, *SL,* receiver gain G_r, frequency response of the transmitter Fr and the ensonified footprint area *A*. The transmission loss *TL* depends on the environmental conditions and the travel distance *R* of the signal to the seabed. It can be written as

$$TL = 2\alpha R + 40\log(R) \quad (2)$$

where α is the absorption coefficient depending on the temperature, salinity, acidity, pressure and frequency *f*. The second term in the Eq. 2 accounts for the energy loss of the signal due to geometrical spreading. The ensonified footprint area *A* is not only affected by the sonar characteristics but also by seabed morphology, i.e. the across-track slope ϵ_y and along-track slope ϵ_x. The ensonified footprint area of the pulse limited regime A_p and of the beam limited regime A_b are expressed by [17]

$$A_p = \Omega_{tx} R \frac{c\tau_{eff}}{2\sin(\theta - \epsilon_y)\cos(\varepsilon_x)} \tag{3}$$

and

$$A_b = R^2 \Omega_{tx} \Omega_{rx} \tag{4}$$

respectively, where c is the speed of sound in water, θ is the beam angle with respect to nadir and τ_{eff} is the effective pulse length. Ω_{tx} *and* Ω_{rx} are the beam opening angles for transmission and reception and can be calculated for a continuous line array with length L by [18]

$$\Omega = \frac{\lambda}{L} \tag{5}$$

where λ is the wavelength of the transmitted signal given by $\lambda = c/f$. Considering a constant array length the beam width changes with varying frequency. Furthermore, the seabed morphology also affects the incident angle of the sound wave on the seabed according to [17]

$$\cos(\vartheta) = \frac{\sin(90 - \theta) + \cos(90 - \theta)\,\epsilon_y}{\sqrt{1 + \epsilon_x^2 \epsilon_y^2}} \tag{6}$$

where ϑ is the incident angle considering the local morphology. The incident angle correction does not change the backscatter value but it assigns to this value the corresponding true incident angle. In environments with a rough seabed morphology, this correction is essential for the Bayesian method for seabed classification.

Accounting for all these factors during the backscatter processing results in relative backscatter strength. To retrieve absolute backscatter strength, it requires a full calibration of MBES systems. However, as long as the relative variation of backscatter strength with respect to varying sediment types and incident angles are preserved within the processing, seabed classification can be carried out.

2.2. Bayesian method

The Bayesian method for sediment classification employed in this paper was first developed by Simons and Snellen [15], where a detailed description of the theory is given, and developed further by Amiri-Simkooei [17]. This section provides an overview of the main concept and

processing steps taken to generate the sediment maps of the multispectral MBES dataset. According to the central limit theorem, backscatter strength can be assumed to follow a Gaussian distribution if a sufficient number of scatter pixels are considered for determining the average (over the beam footprint) backscatter strength [15]. A scatter pixel represents the instantaneously ensonified area of the seafloor by the transmitted pulse of the MBES, i.e. the signal footprint. If the frequency and angle of incidence are constant, the backscatter strength is dependent on the seabed properties. Thus, if the survey area contains *m* different sediment types, with specific seabed properties, the backscatter histogram of a selected oblique beam of a MBES can be represented by a combination of *m* Gaussian distributions. The model of the histogram for measured backscatter values per beam can be expressed as

$$\mathrm{f}(\mathrm{y}_j \,|\mathbf{x}) = \sum_{k=1}^{m} c_k \exp\left(\frac{\left(y_j - \bar{y}_k\right)^2}{2\sigma_{y_k}^2}\right) \tag{7}$$

with y_j the j^{th} backscatter value in the histogram ($j=1,\ldots,M$, with M the total number of bins in the histogram). $\boldsymbol{x}$ is the vector containing the unknown parameters: $\mathbf{x} = (\bar{y}_1, \ldots, \bar{y}_m, \sigma_{y1}, \ldots, \sigma_{ym}, c_1, \ldots, c_m)$ with $\bar{y}_k$ the means, σ_{y_k} the standard deviations and c_k the strengths of the Gaussian distributions. The unknown parameters are determined by fitting the modelled histogram to the measured histogram. In order to determine the optimal number of Gaussians, the χ^2 goodness of fit test (Chi-square test) can be used, where χ^2 is defined as

$$\chi^2 = \sum_{j=1}^{M} \frac{\left(n_j - f\left(y_j \mid X\right)\right)^2}{\sigma_j^2} \tag{8}$$

where n_j denotes the number of measurements per bin of the aforementioned histogram. For n_j a Poisson-distribution is postulated. The variances σ_j^2 are thus equal to n_j. The goodness of fit statistic is χ^2 distributed with $v = M - 3m$ degrees of freedom. The goodness-of-fit criterion is then further defined as the reduced-χ^2 statistic ($\chi_v^2 = \chi^2/v$) having a value close to one for a good fit, indicating that the differences between modelled and measured histogram fall within the uncertainties of the measurements. The value of m for which a further increase of m does not generate a significantly better fit of the model to the histogram, as quantified by the reduced-χ^2 measure, is taken to be the number of seafloor types that can be discriminated in the survey area based on the backscatter data.

The actual classification is based on the Bayes decision rule. In accordance with the χ^2 test m states or hypotheses, indicated as $H_{k,}\ k = 1, \ldots, m$ exist. These hypotheses correspond to the m seafloor types present in the surveyed area. In the following, the Bayesian decision rule for multiple hypotheses is used to define which hypothesis is accepted, i.e.

$$\text{accept} \quad H_k \quad if \quad \max\{f(y_j|H_i)P(H_i)\} = f(y_j|H_{k)})P(H_k) \tag{9}$$

where $P(H_i)$ is the a priori probability of hypothesis H_i with $i = 1,\ldots,m$. Considering that the measurements are taken for the first time, all hypotheses are equally likely, which results in $P(H_i)=1/m$. In that regard, the decision rule can be simplified to

$$\text{accept} \quad H_k \quad if \quad \max\{f(y_j|H_i))\} = f(y_j|H_{k)}). \tag{10}$$

That means, the hypothesis is selected which maximizing the likelihood $f(y_j|H)$ for the observation y_j. Therefore, the intersections of the m Gaussians have to be determined which results in m non-overlapping acceptance regions A_k defining the so-called acoustic classes. The Bayes decision rule enables the calculation of the probabilities of incorrect decision β_{ki}. The overlap between the Gaussian distributions represent the area of incorrect decisions (i.e. misclassification). Statistically, β_{ki} denotes the probability that H_k is true but H_i is choosen and can be expressed as

$$\beta_{ki} = \int_{A_i} f(y|H_k)dy. \tag{11}$$

The values of β_{ki} are contained in the so-called decision matrix and can be used to evaluate the probability of misclassification

2.3. Multispectral seabed classification

In this study, the decision matrix is employed to evaluate the benefit of using additional frequencies to increase the discrimination performance of seabed classification methods. According to the Bayes method, each Gaussian distribution obtained from the classification of a single frequency MBES dataset represents a sediment type with specific sediment properties. However, only those sediment types that shows up as different sediment types at the applied frequencies can be distinguished. That means that if two different sediment types have highly

similar acoustic signatures, they will be represented by the same Gaussian. In general, different frequencies show different discrimination performance (see Section 1). Therefore, applying the Bayesian technique to three MBES datasets acquired in the same area with three different frequencies might reveal acoustic classes which do not necessarily represent the same sediment type or properties. The spatial correlation between the acoustic classes as obtained for the different frequencies provide an estimate of the additional information gathered by the use of different frequencies. To account for the known probability of misclassification, the information contained in the decision matrix is accounted for when combining the classification results as obtained from the different frequencies.

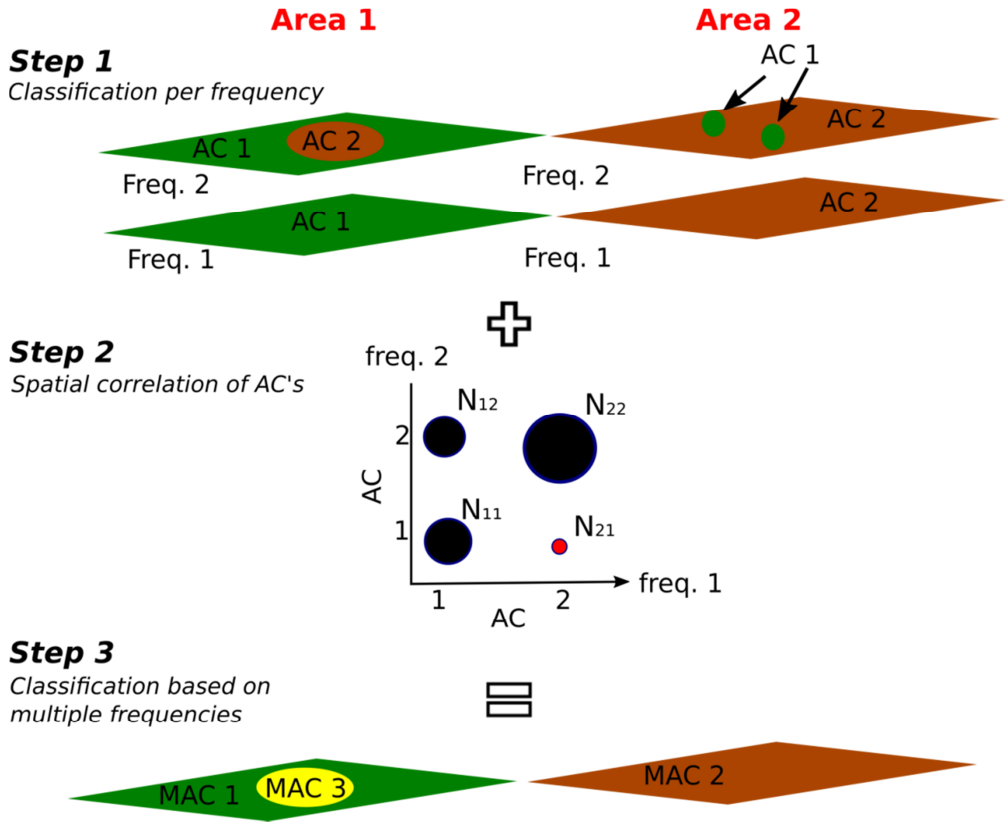

Fig. 1 Sketch of the workflow for multispectral seabed classification based on the Bayesian method. Step 1 represents the application of the Bayesian method to each frequency separately. Step 2 is the correlation of the AC's obtained from different frequencies while accounting for the probability of misclassification. AC combinations indicated with black dots are proven as reliable by the validity check (see Eq. 12) and thus determine the three new multispectral acoustic classes (MAC). Whereas the combination indicates with a red dot is discarded. Step 3 represents the final map production based on the results of step 2 and the assignment of the new MAC's.

To statistically assess the actual existence of classes that are revealed solely by combining the classification of different frequencies, the probability of misclassification is used. If the validity

check is accepted each remaining and a statistically reliable combination of acoustic classes represents a new class, which is called multispectral acoustic class (MAC). In the following the validity check is explained by considering two frequencies f_1 and f_2 and two acoustic classes AC 1 and AC 2 as it is displayed in Fig. 1. For the combination of AC 1 and AC 1, the validity check can be written as follows

$$accept\ MAC \quad if\ \frac{N_{11}}{N_{11}+N_{12}} > 1-(\beta_{11})_{f_1}(\beta_{11})_{f_2} \quad or\ \frac{N_{11}}{N_{11}+N_{21}} > 1-(\beta_{11})_{f_1}(\beta_{11})_{f_2} \quad (12)$$

where N_{11} is the number of times that the combination of AC 1 and AC 1 for f_1 and f_2, respectively, occur in the survey area (see Fig. 1). N_{12} is the number of times that the combination of AC 1 and AC 2 for f_1 and f_2, respectively, is occurring. N_{21} is the number of times that the combination of AC 2 and AC 1 for f_1 and f_2, respectively, is occurring. $(\beta_{11})_{f_1}$ is the probability that AC 1 as obtained at f_1 is successfully classified (see Eq. 11).

From Eq. 12 it follows that, if the percentage occurrence of the combination of AC 1 and AC 1 of the different frequencies is larger than the probability of this combination occurs purely due to the probability of misclassification, then the combination is accepted as statistically reliable. Additional information are obtained by using different frequencies if more reliable combinations than the number of acoustic classes per frequency exist (Step 2 of Fig. 1). The procedure needs to be carried out for all AC's and frequencies to determine all MAC's.

3. Study area and dataset

3.1. Bedford area

The dataset used in this paper was acquired in the Bedford Basin, Halifax, Nova Scotia by a broadband MBES (R2Sonic 2026), which allows the operating frequency to be modified on a ping-by-ping basis. The data were collected at three different frequencies (100 kHz, 200 kHz, 400 kHz). The MBES was pole-mounted on the MV Eastcom. The MBES backscatter is stored as a single value of backscatter intensity per beam representing the return level at the bottom detection point and as a time-series per beam representing the scatter pixels [16]. In this study, the backscatter intensities per beam are considered. The MBES data covers an area of approximately 1.84 km^2 and the water depth ranges between 13 m to 85 m (Fig. 2). A total of 12 lines were surveyed with approximately 50% overlap. Further, georeferenced video footage were

collected within the survey area using a drop-down underwater camera frame fitted with a Sub-C underwater camera and lights. The selected area comprises of sediment types ranging from bedrock to silt with underlying harder substrata. In addition, different types of benthic flora and fauna are visible in the video footages. As reported in [11], the deeper area consist of soft mud and partly covered with various benthic flora. Close to the harbor (SW in Fig. 2), the area comprised a mixture of hard substrata such as bedrock and boulders with attached epifauna. The morphology of the NE area contains settlements of soft sediments and several features which are caused by disposal of dredge spoils [11]. This Bedford Basin is chosen for the acoustic classification because it has two datasets from different years, 2016 and 2017, which enables the comparison and verification of the backscatter processing.

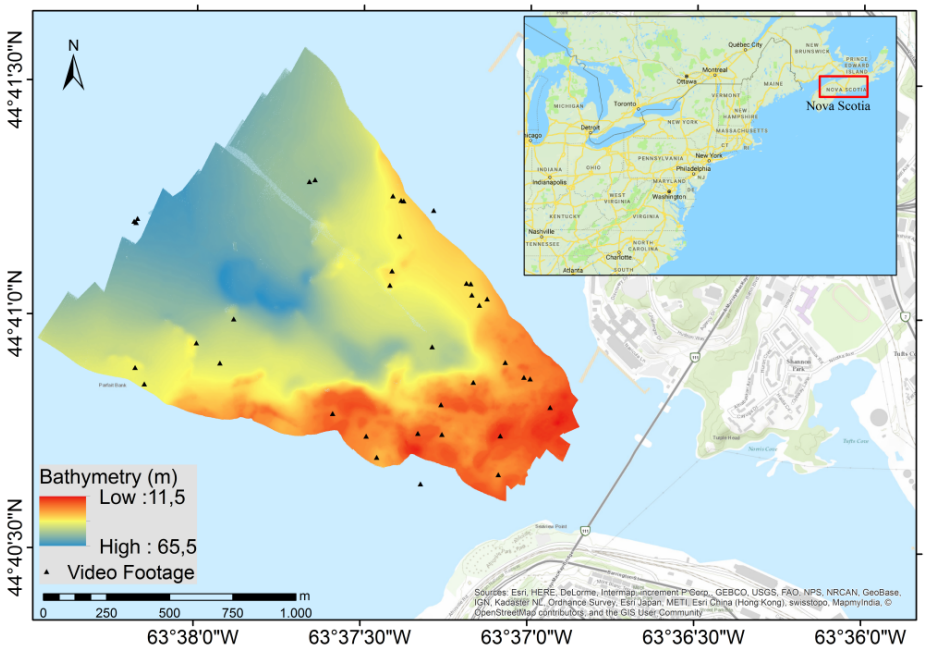

Fig. 2 Bathymetry and location of the survey area (Bedford Basin, Canada). The displayed MBES bathymetry was acquired in 2016.

3.2. Multispectral data

Bathymetry and backscatter data were collected with the R2Sonic 2026 MBES which was configured to collect data at frequencies of 100, 200 and 400 kHz on sequential pings with operating settings tuned to achieve full coverage across these frequencies. As system settings such as transmit power, gain and pulse length are all accessible to the user or predefined in automatic acquisition modes, varying acquisition parameters occur in the employed dataset.

Table 1 shows the technical characteristics of the R2Sonic 2026 MBES and some parameters used during the acquisition.

Table 1. Characteristic of R2Sonic 2026 MBES used during acquisitions.

Frequency	100 kHz, 200 kHz, 400 kHz
Number of beams	256
Beam width (Ω_{tx}x Ω_{rx})	2° x 2° (100 kHz), 1° x 1° (200 kHz), 0.5° x 0.5° (400 kHz)
Swath coverage	~ 65° for starboard and port side
Nominal pulse Length τ_n	150 µs
Pulse type	Shaped CW
Ping rate	Up to 60 Hz
Receiver Bandwidth B	7500 Hz
Positioning & motion compensation	POS MV Wave Master Inertial Navigation System (INS)
Sound velocity device	Valeport and AML Base X2

4. Results

4.1. Backscatter correction

The multi-frequency MBES datasets, acquired in the Bedford Basin in 2016 and 2017, are utilized in this study. Both are subject to changes in source level, receiver gain and a so-called "spreading coefficient loss term" [19] across the entire survey area. In addition, a correction term for the source level to account for the difference in requested versus actual source level was introduced by R2Sonic. Clearly, the freedom and flexibility given by this MBES system to change the settings provide some advantages, for example to stay within the dynamic range and to receive sufficient acoustic energy, but it also complicates the acoustic data processing and may critically affect the backscatter measurements. According to Eq. 1, the received echo level EL is corrected for the actual source level SL and the receiver gain G_r (stored G_r is multiplied by 2 (according to R2Sonic). R2Sonic MBES's compensate for the transmission loss TL already during acquisition. However, the absorption coefficient α and the so-called "spreading coefficient loss term" used by the MBES are replaced with physical reasonable values according to Eq. 2. A more appropriate α is estimated using the model of Francois and Garrison [20], [21] and finally integrated over the depth. The environmental variables of the water column

(temperature, pressure and salinity) are received from measured CTD profiles and a pH-value of 8 is assumed for the calculation. α is highly frequency dependent and a reliable calculation is essential for the backscatter processing in general but, in particular, for multispectral backscatter data. The values for α and "spreading coefficient loss term" used by the MBES and used in this study for the backscatter correction are displayed in Table 2

Table 2. The absorption and "spreading coefficient loss term" (spread.) stored in the datagram and the used value in the backscatter processing.

	100 kHz α [dB/km]	200 kHz α [dB/km]	400 kHz α [dB/km]	100 kHz spread. [-]	200 kHz spread. [-]	400 kHz spread. [-]
stored Bedford 2016	80	80	80	30	30	30
stored Bedford 2017	23	40	0	35	30	35-55
used Bedford 2016	23.2	39.4	91.6	40	40	40
used Bedford 2017	23.3	39.5	91.9	40	40	40

The R2Sonic MBES stores backscatter intensities and backscatter time series in digitized pressure units with an unknown scaling due to lacking calibrations. The backscatter intensity values per beam are converted to decibel values. Due to lacking calibrations the converted backscatter values are unrealistically high as indicated by positive decibel values. Even though the relative difference in backscatter is correct, indicated by reliable ARC for specific sediments (Fig. 3), a backscatter correction term of 100 dB is added to obtain realistic backscatter values. This value is retrieved by comparing the APL-model results with the measured ARC curves from a muddy area per incident angle (Fig. 4 and Fig. 3, respectively). Furthermore, a frequency response correction term *FR* is added to the received signal intensity (see Eq. 1) to compensate for the acoustic response of the transmitter for the different frequencies. The frequency response calculations are a theoretical approximation based on measured transducer characteristics (M. Brissette 2018, personal communication, 12. Januar). In addition, the received signal is compensated for the ensonified footprint area *A* to retrieve relative backscatter strength according to Eq. 1, 3 and 4. This step is also frequency dependent due to the dependency of the widths Ω_{rx} and Ω_{tx} on the wavelength λ of the transmitted signal (see Eq. 5). The beam widths for the three frequencies are displayed in Table 1. In the pulse limited regime the calculation of the footprint area A_p requires the effective pulse length τ_{eff} (see Eq. 3). It differs from the

nominal pulse length τ_n due to the applied trapezoid filter aiming to suppress spectral leakage. In this study, it is assumed that the given receiver bandwidth B stored in the datagrams represents the width of the main lobe of the time series signal in the frequency domain at the reception. Considering this assumption, τ_{eff} can be calculated by $\tau_{eff} = \frac{1}{B}$ (Table 2). This results in τ_{eff} of 133 µm, a decrease of 12% compared to τ_n. The ensonified footprint area calculation also requires the consideration of the local topography which influences the incident angle ϑ (see Eq. 3). The required across-track ϵ_y and along-track slopes ϵ_x are calculated with respect to the heading of the vessels. Finally, the true incident angle ϑ is calculated from the beam angle θ and the along- and across track slopes using Eq. 6.

The result from the described processing steps is the backscatter strength BS as a function of incident angle, also known as angular response curve (ARC). To proof the reliability of the backscatter corrections, the ARC's from areas assumed to be relatively homogeneous measured in 2016 and 2017 are compared. The approach here is to use data from two different areas of sediments, i.e. muddy (area 1) and gravel, boulder (area 2). The results are displayed in Fig. 3. For the majority of the incident angles, the backscatter values of the three frequencies agree within less than 1 dB. Except for lower incident angles and around nadir the deviation is up to maximum 3 dB. This is explained due to noisy backscatter data at nadir caused by the specular reflection and that the track lines are not exactly at the same location. In that regard the same incident angle does not necessarily sense the same sediment and, in addition, lower incident angles are more affected being more sensitive to sediment changes (see Fig. 4). In conclusion, the backscatter correction appears to be successfully applied.

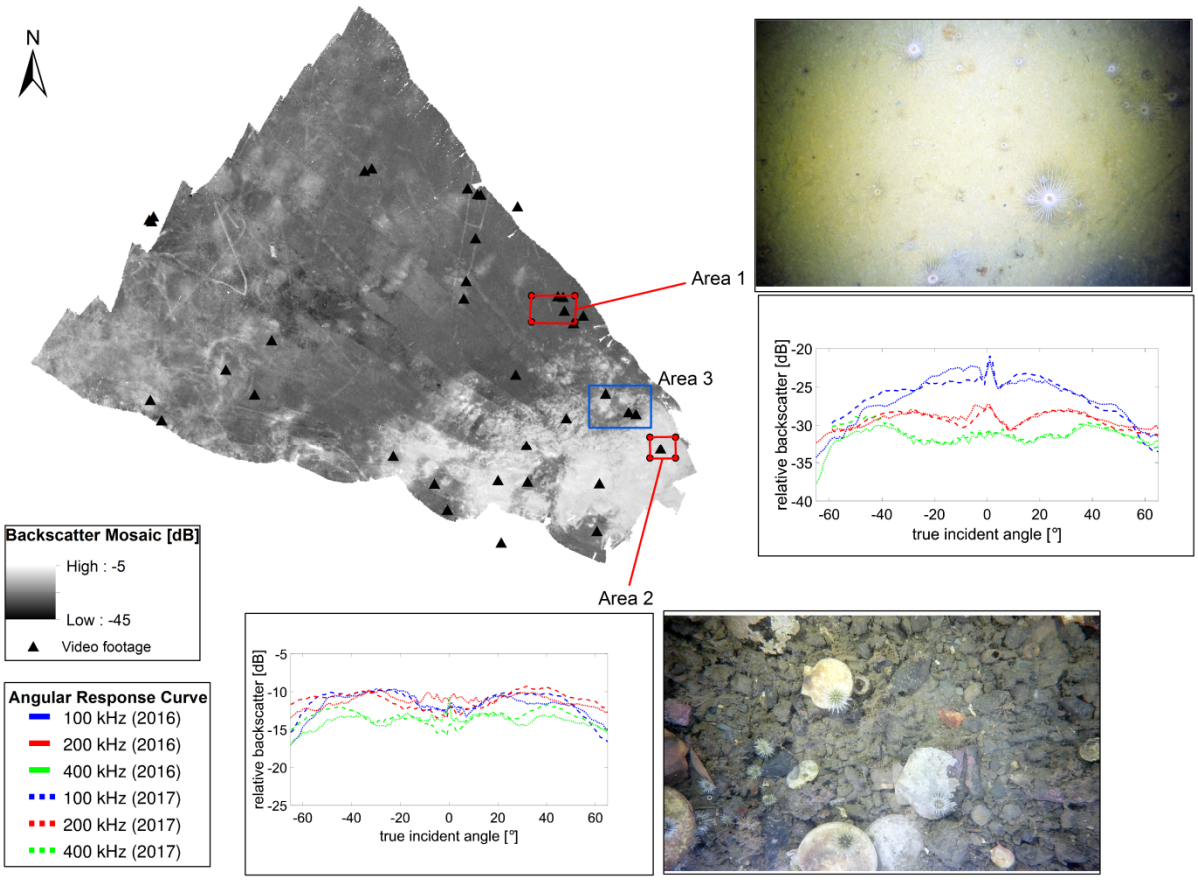

Fig. 3 Comparison of the processed angular response curves (ARC) of two different sediment types retrieved from the multispectral MBES dataset acquired in 2016 and 2017 in the Bedford Basin. Area 1 indicates a muddy sediment and Area 2 indicates gravel to boulders. The displayed backscatter mosaic (200 kHz, 2016) has a spatial resolution of 2 m by 2 m.

The shape of the ARC corresponding to area 2 at 200 and 400 kHz is very flat suggesting a rough seabed with respect to the wavelength. The ARC of 100 kHz is similar except for a significant decrease in backscatter for incident angles larger than 40° at 100 kHz indicating an acoustically smoother seabed. The relatively flat ARC including a missing near-nadir peak can be explained by the APL-UW (1994) model (Fig. 4), where backscatter strength at 100 kHz for a gravelly area do not have a high variation for all incident angles. In area 1, the absolute backscatter value is significantly lower compared to area 2 at each frequency, indicating a softer and smoother seabed which is confirmed by the video footage showing gravel, boulders and soft sediment, respectively. The shape of the ARC's appear to differ. The 100 kHz ARC has a near-nadir peak with a decrease in backscatter with increasing incident angles as expected from the APL-UW (1994) for fine sediments (Fig. 4). The flatness of the ARC's shapes increases from

200 to 400 kHz indicating that the seabed appears rougher with increasing frequency. In essence, the ARC curves show higher acoustic sensitivity per frequency for softer sediments.

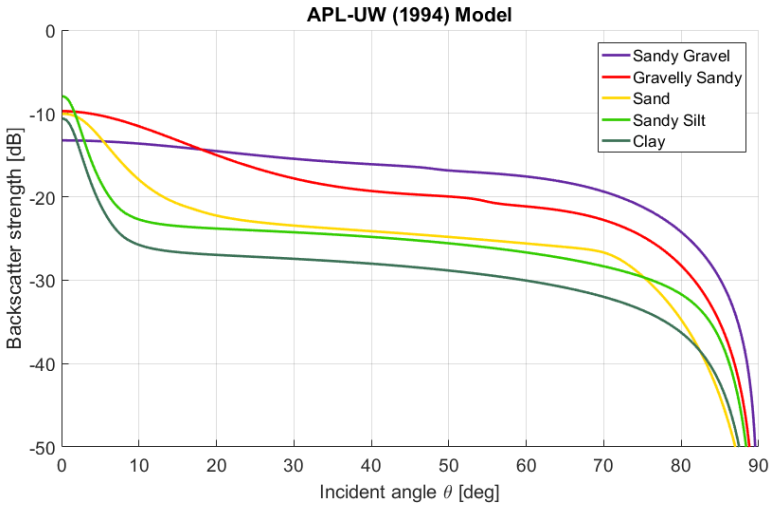

Fig. 4 Angular response curves calculated with the APL-model at 100 kHz [5].

Backscatter mosaics are generated by correcting for the angular dependency using the local Z-score approach with a sliding window of 100 pings and the averaged backscatter value from 30° to 60° (Fig. 5) [22]. No despeckle or anti-aliasing filters are applied to the mosaics to keep the mosaics as unfiltered as possible for the verification of the backscatter processing. Some along-track artefacts are visible, which are probably induced by the local angular correction due to seabed changes in across-track direction [23]. However, they do not affect the acoustic classification based on the Bayesian method (backscatter is considered per beam separately (see Section 2.2)). Still, the backscatter mosaics indicate a reliable backscatter processing. The backscatter mosaics show clearly different spatial pattern indicating varying sensitivities at the three frequencies for different seabed types. The most spatial variety is visible at 100 kHz.

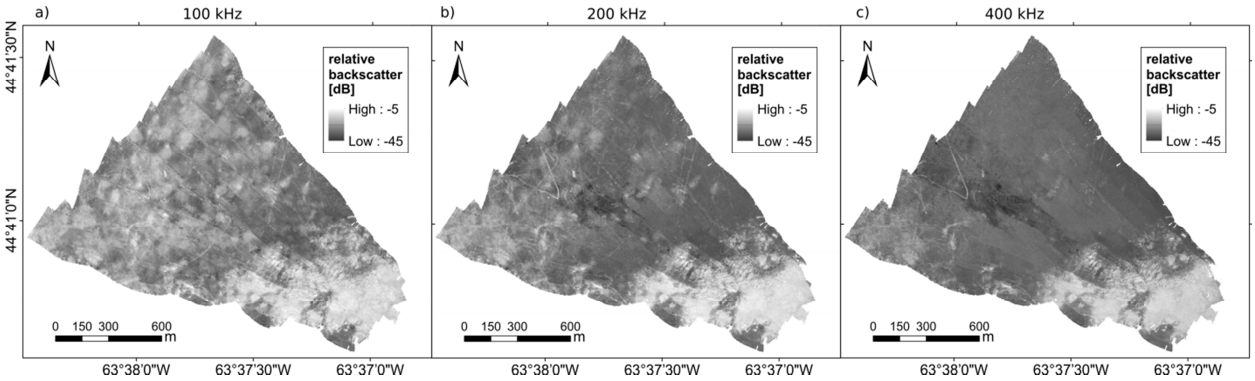

Fig. 5 Backscatter mosaics obtained from a) 100 kHz, b) 200 kHz and c) 400 kHz. The spatial resolution is 2 m by 2 m. Local Z-score with a sliding window of 100 pings is used to correct for the angular dependency [22].

4.2. Application of the Bayesian method to multispectral backscatter

The Bayesian method is applied to the relative backscatter strength at each frequency separately. Because of the high seabed morphology, the backscatter values per true incident angle are considered in this work. The first step is to average the backscatter values over a range of pings and incident angels to ensure the assumption of normally distributed backscatter to be valid according to the theory of the Bayesian method (Section 2.2). Accounting for the dependency of the number of scatter pixels per beam, the size of the averaging window in across-track direction increases from 1.2° to 5° with decreasing incident angle and in the along-track direction from 1 to 4 pings with increasing water depth.

The next step involves the identification of the optimal number of classes by fitting Gaussian distributions to the measured backscatter histogram per incident angle (according to Eq. 7). Fig. 6 displays the measured histograms from the 55° (+/- 0.6) incident angle (starboard side) at 100, 200 and 400 kHz, as an example.

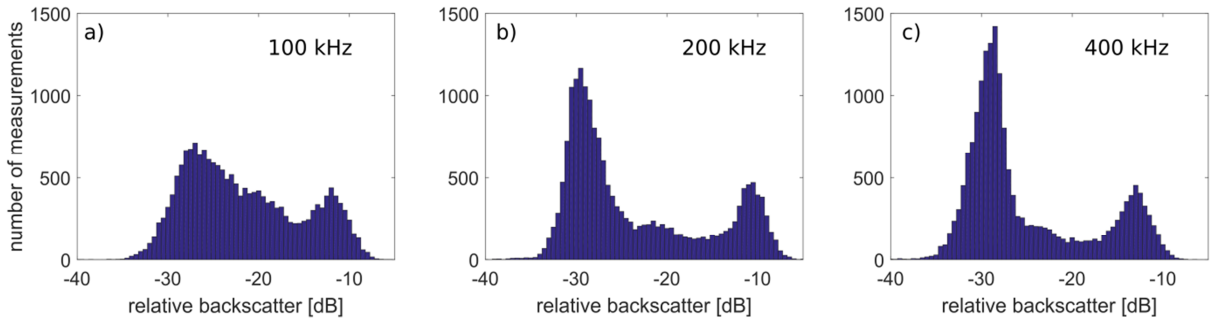

Fig. 6 Histogram of measured backscatter obtained from the incident angle range 53.4-54.6 degrees (~54 degree) for the full survey area. a) 100 kHz, b) 200 kHz and c) 400 kHz.

The outer beams are preferably utilized for fitting the Gaussians, and hence identifying the number of classes. First of all, larger incident angles include more scatter pixels per area, lowering the Gaussian's standard deviation and consequently provide increased geoacoustic resolution (see section 2.2). Second, the incident angles between 30° and 70° provide the most discrimination potential. This is displayed in Fig. 4 where the backscatter strength is expressed as a function of incident angles.

However, incident angles greater than 60° are found to hold very low backscatter strength values and tend to be noisy. Accounting for these issues in the present datasets and to receive a robust statistical estimate, a range of incident angles (considering the local topography) from 40° to 57° degrees are selected as most suitable and used for estimating the optimal number of acoustic classes per frequency. The Chi-square test as applied to the incident angles from 40° to 57° of the starboard and port side at 100, 200 and 400 kHz are displayed in Fig. 7.

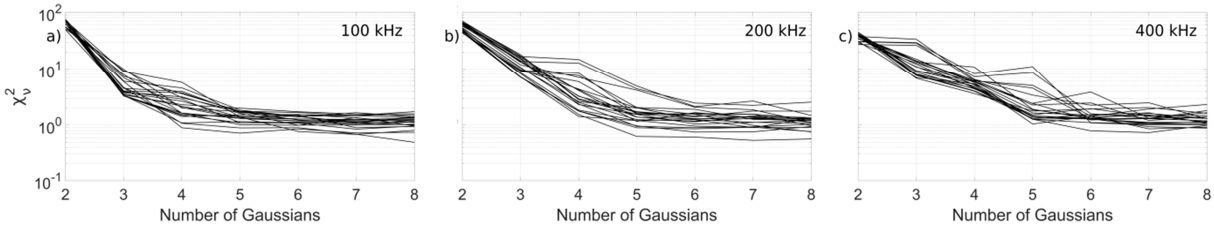

Fig. 7 Chi-square test applied to a) 100 kHz, b) 200 kHz and c) 400 kHz for incident angles from 40° to 57°.

A visual inspection of the results of the Chi-square tests already indicates an optimal fit to the measured histograms of 4 Gaussians for the 100 kHz dataset and 5 Gaussians for the 200 and 400 kHz dataset, respectively. Furthermore, an objective evaluation of the Chi-square values

accounting for the improvement of the fit versus the increase of the number of Gaussians yields to a majority suggesting 4 Gaussians for 100 kHz and 5 Gaussians for 200 and 400 kHz, respectively (see Section 2.2). To further demonstrate the validity of the results, the fits of the modelled Gaussian distributions to the measured histograms of the 54° incident angle are displayed in Fig. 8. Fig. 8 a) and b) show that an increase from 4 to 5 Gaussian distributions does not improve the fit to the measured backscatter data at 100 kHz. In contrast, the representation of the measured backscatter of 200 and 400 kHz is significantly improved by using 5 instead of 4 Gaussian distributions. These findings are observed for the majority of the considered angles. The results indicate that the frequencies of 200 and 400 kHz are able to discriminate one more class compared to 100 kHz in this study site. Even though it is decided to select 5 classes for 200 and 400 kHz, the Chi-square test, shown in Fig. 8 b) and c), indicates that 200 kHz reaches lower Chi-square values slightly earlier than 400 kHz indicating higher discrimination for 400 kHz.

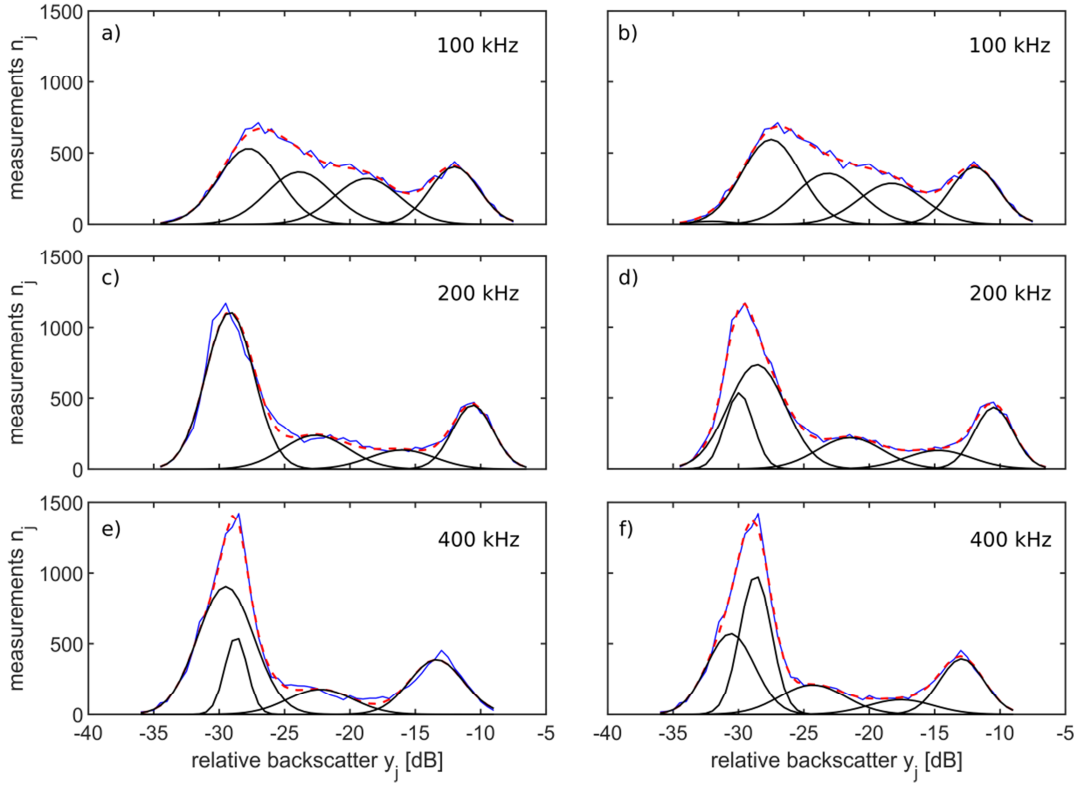

Fig. 8 Model fits to the histogram of the measured backscatter data $\boldsymbol{n_j}$ (blue) per 0.5 dB bin $\boldsymbol{y_j}$ at a, b) 100 kHz, c, d) 200 kHz and e, f) 400 kHz are displayed. The modelled $\boldsymbol{f(y_j|x)}$ histogram calculated by using a, c, e) 4 Gaussian distributions and b, d, f) 5 Gaussian distributions is shown in red. The corresponding Gaussians are displayed in black.

For the generation of the final acoustic class maps the incident angles from 10° to 60° are considered. The backscatter data around nadir are prone to specular reflection and therefore too noisy to provide reliable classification. The final acoustic class maps for 100, 200 and 400 kHz are displayed in Fig. 9.

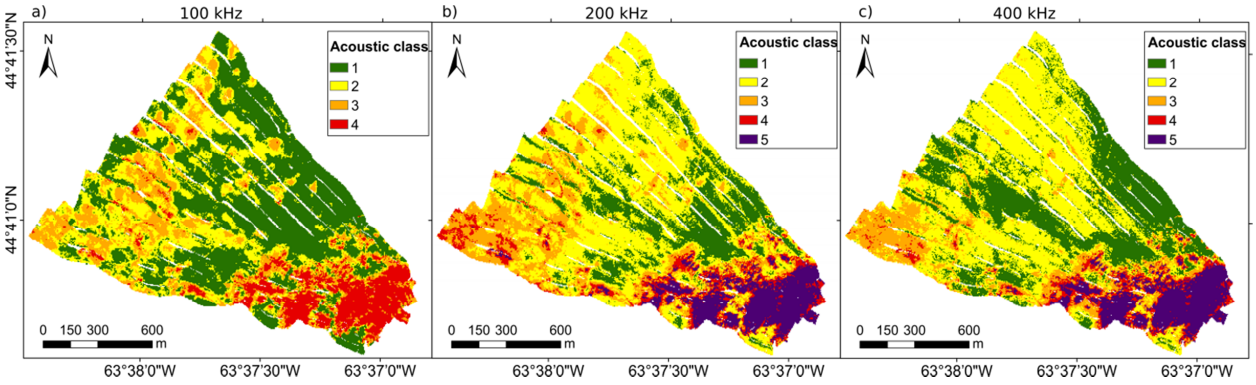

Fig. 9 Acoustic classification maps for a) 100 kHz, b) 200 kHz and c) 400 kHz. The spatial resolution is 5 m by 5 m. White spots indicate no data caused by neglected backscatter data at nadir.

The SE part of the study area shows the same spatial structures in each classification map. In particular AC 4 at 100 kHz and AC 5 at 200 and 400 kHz cover this SE part of the seabed indicating a correlation with the same seabed type. The acoustic classification of the NW area demonstrates different spatial patterns, in particular between 100 and 400 kHz. In Fig. 9 a) and partly in Fig. 9 b) circular to elongated features are visible and classified as AC 3 in 100 and in 200 kHz. However, in the maps of 100 kHz these features are more pronounced. In the 400 kHz map the features are not apparent and the locations are classified as AC 2 or AC1 like the surrounding seabed. A second noticeable difference between the acoustic classification maps is the spatial distribution of AC 2 and AC1. AC 2 (yellow) covers a large area in the northern part of the 200 and 400 kHz map compared to a very limited extent of AC 2 and a larger extent of AC 1 in the 400 kHz map. This indicates that AC 1 and AC 2 of 100 kHz represent different seabed properties than AC 1 and AC 2 of 200 and 400 kHz. In general, the most differences are visible between the ASC maps obtained at 100 and 400 kHz.

4.3. Evaluation of the benefit using multiple frequencies

To evaluate the information content of each frequency and the additional information by combining different frequencies, the spatial correlation between the individual AC's obtained from the different frequencies are calculated (see section 2.3). In general, almost all AC's

combinations are more or less present (it is not shown here). To determine which combinations are significant and do not occur due to misclassification, Eq. 12 is used to reveal the statistically reliable correlations (see Section 2.3). The accepted combinations are visualized in Fig. 10. The size of the circles represents the number of times that a particular combination occurs in the survey area. The larger the circle the higher the number of locations where the AC's are in agreement.

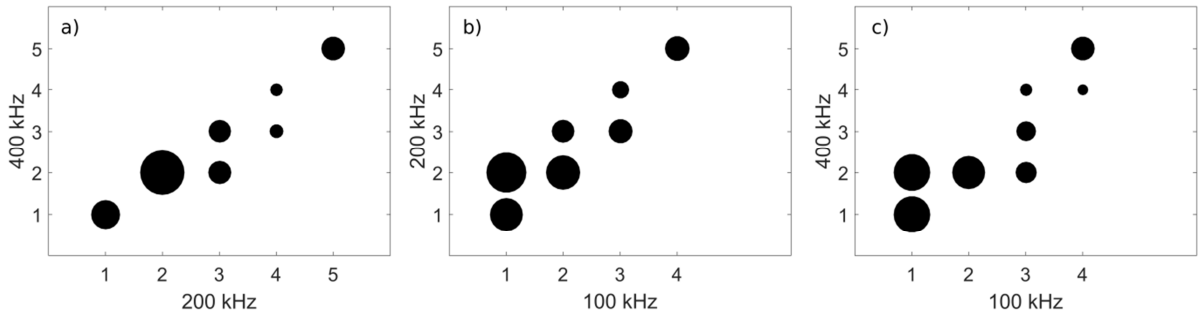

Fig. 10 Correlation plot of a) 400 and 200 kHz, b) 200 and 100 kHz and c) 400 and 100 kHz. The size of the circles represent the number of the AC's combination occur in the survey area. To obtain theses plots Step 1 and 2 described in Section 2.3 are applied.

The benefit of using more than one frequency can be identified if an AC obtained from one frequency correlates to more than one AC of the other frequency. The correlation plot of 200 and 400 kHz (Fig. 10a) shows a strong correlation between the same AC's. In addition, two more combinations are obtained (AC 2/3, AC 3/ 4; 400/200 kHz). In Fig. 10 b) there are two additional combinations represented by AC 2 and AC 1 as well as AC 3 and AC 2 from 100 and 200 kHz, respectively. However, in Fig. 10 c) there are three additional and clearly separated combinations visible (AC 2/ 1, AC 2/ 3, AC 4/3; 400/100 kHz). In essence, the most statistically reliable combinations (equal to 8, see Fig. 10c) are obtained from the correlation of the AC's of 100 and 400 kHz. This indicates that most of the information about the seabed in this study area can be retrieved from 100 and 400 kHz. This confirms the visual interpretation of Fig. 9.

4.4. Combination of multiple frequencies

In this section the information provided at each frequency are combined with the aim to generate a multispectral acoustic classification map. The general workflow consists of three steps which are displayed in Fig. 1. Step 1 and 2 are carried out in Section 4.2 and 4.3. In the final step 3, the new multispectral acoustic classes (MAC's) are defined from the statistically reliable combinations of the original AC's obtained per frequency. Each combination representing a

unique information about the seabed properties are considered as a new MAC yielding to 9 MAC's in total (Fig. 11) (see section 4.3). The data points considered as unreliable in step 2 are not assigned to a MAC. Therefore, the coverage of the final map is slightly less compared to the maps of the single frequencies.

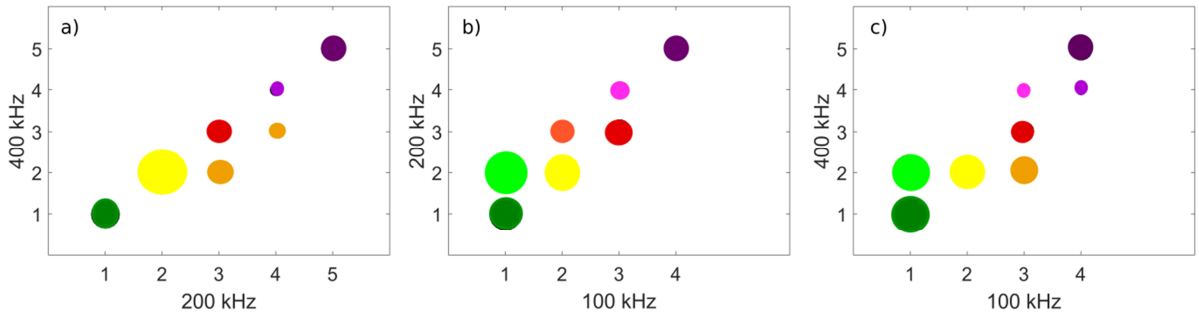

Fig. 11 Definition of MAC by using the reliable combinations of AC's obtained from the three frequencies. MAC revealed by the AC' combinations of a) 400 and 200 kHz, b) 200 and 100 kHz and c) 400 and 100 kHz. The colors indicate the different MAC's. The corresponding legend is displayed in Fig. 12.

The final multispectral acoustic classification map considering the 9 MAC is shown in Fig. 12 Multispectral acoustic classification map obtained from the combination of the individual single frequency maps (Fig. 9). The spatial resolution is 5 m by 5 m.. The different spatial patterns observed in each of the acoustic classification maps (100, 200 and 400 kHz, Fig. 1) are now all visible in the combined map. The circular to elongated features mainly visible in the 100 kHz map and less pronounced in the 200 kHz map are clearly visible in the combined map. In addition, they are now distinguishable from the major high acoustic class structure in the SE of the study area and from the structure in the NW which are assigned to the same AC as the circular structures in the 100 and 200 kHz map. Also the SW-NE stripe (according to Brown *et al.* [6], these features represent trawl marks) are clearly distinguished in the final map from the surrounding seabed. This feature is only clearly visible in the 100 kHz and slightly in the 200 kHz map but doesn't show up in the 400 kHz map. The softer sediments (lower AC and lower backscatter, respectively) show a higher discrimination in the final MAC map. AC 1 of 100 kHz (dark green in Fig. 9a) and AC 1 and AC 2 of 200 and 400 kHz (dark green and yellow in Fig. 9b and c) are converted to three separated MAC's in the final map indicating a reliable geological spatial pattern. However, it has to be mentioned that the combined map appears to be slightly noisier. One major reason is that the noise inherent in each of the original maps caused by remaining

backscatter artefacts or misclassification propagates and amplifies into the final map. Another reason is that 9 classes exhibit a higher total probability of misclassification than the 4 or 5 classes at the single frequencies.

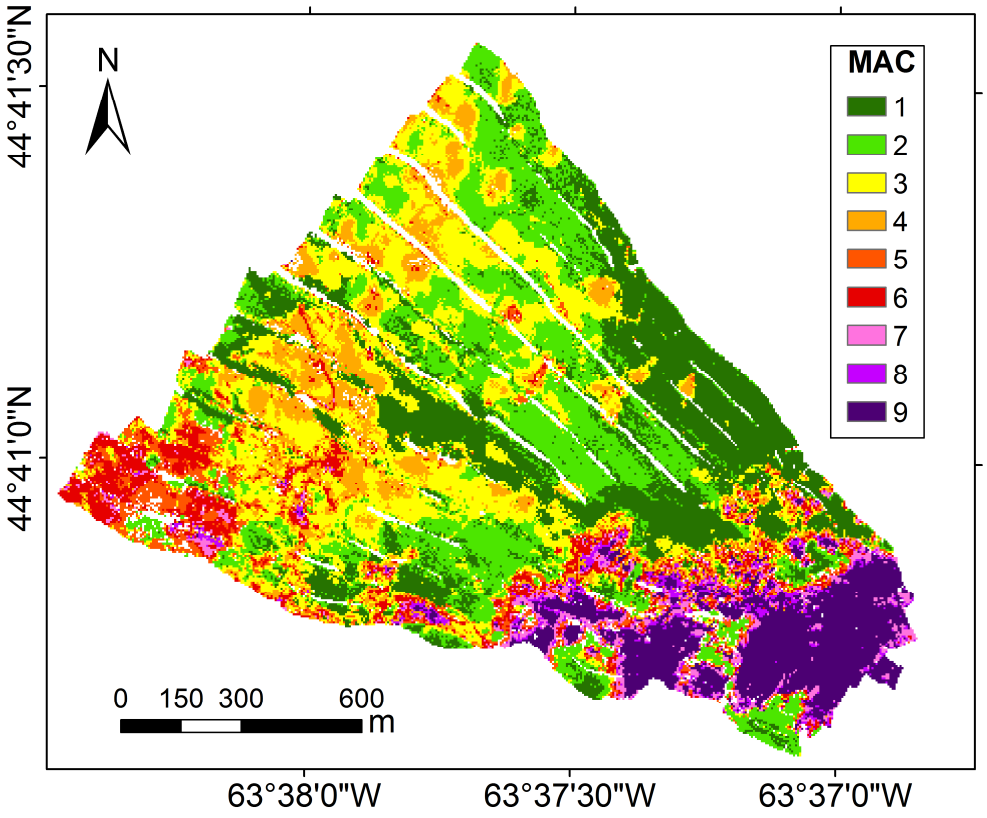

Fig. 12 Multispectral acoustic classification map obtained from the combination of the individual single frequency maps (Fig. 9). The spatial resolution is 5 m by 5 m.

4.5. Correlation analysis of ground truth and acoustic classes

In this section the results of the Bayesian technique are quantitatively and qualitatively compared to the video footage with three aims: 1) correlate AC and MAC to sediments or seabed features, 2) produce a sediment map from the AC and MAC map and 3) verify the benefit of using multi frequencies. For the qualitative comparison the seabed visible on the video footage is categorized into distinct classes. Three video footage categories are chosen: soft, mixed and hard. “Hard” represents all areas where the entire area is covered with boulders, shells or gravel (e.g., video footage sample S1 in Fig. 14). “Mixed” displays areas where a mixture of soft sediments and boulders are observed (e.g., video footage sample S4 in Fig. 14). “Soft” contains all areas where soft sediments are present (e.g., video footage samples S3 and S2 in Fig. 14). A finer distinction

of the category “soft” is not carried out due to following reasons: i) a clear distinction between mud, silt or fine sand is not feasible on the basis of the existing video footage, ii) the amount and consistency of benthic flora and fauna or gas releases vary significantly. The grain size and the coexistence with benthic flora and fauna as well as gas seeps can highly influence the backscatter strength [13], [24], [25], [26]. The significance of the grain size is also indicated by the modelled backscatter strength in Fig. 4. All this would hamper a reliable comparison to the acoustic classification results with a finer distinction than three categories.

The correlation of AC’s and MAC’s with the three video footage categories are displayed in Fig. 13, in which the mode (most frequently occurring value) of the AC’s in a radius of 10 m around the video footage is calculated and compared to the video footage. For all frequencies there is a correlation of AC 1 and AC 2 with the soft sediment class and a good correlation of the highest AC with the hard substrata. However, AC 3 represents mostly the soft substrata but also occurs in the mixed category. In general, the mixed category is distributed over the intermediate to the highest classes. Considering the MAC results there is no improvement compared to the single frequencies observed.

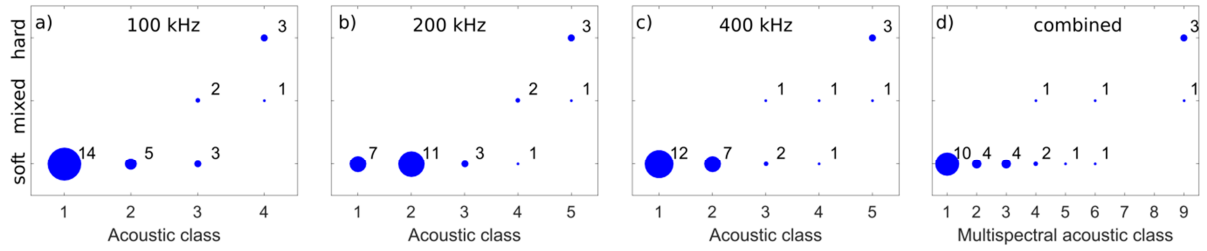

Fig. 13 Correlation plot of video footage category (soft, mixed, hard) with AC’s and MAC’s obtained from the Bayesian classification. Numbers indicate how often the categorized video footage samples (see Fig. 2) are represented by a specific AC or MAC.

Because of the complex seabed and, therefore, the relatively coarse distinction of the video footage in only three categories, a more detailed comparison of the classification results and the video footage is carried out in Fig. 14 and Fig. 15. Clearly, the highest AC (AC 4 for 100 kHz, AC 5 for 200 and 400 kHz and MAC 9 for the combined map) represents a seabed extensively covered with boulders, shells, and gravel, as indicated by video footage sample S1 (sample means here the location of the video footage). The sample S4 displays a mixture of boulders (coral reef) with soft sediments. In the AC map of 100 kHz (Fig. 14a) the sample S4 has the same AC as sample S1. In the 200 and 400 kHz map, the sample is located at the second highest

AC (i.e. AC 4), separating the seabed type of S1 from S4. Due to the combination of the different frequencies, the MAC also indicates a different seabed type. The sample S2 and S3 are assigned to the soft sediment category in Fig. 13, but a more detailed observation indicates differences in the seabed composition. S2 consists of a soft sediment slightly covered with benthic flora, whereas S3 consists of soft sediments combined with some different benthic flora as well as benthic fauna and gas seeps. In the 100 and 400 kHz maps they are clearly separated by at least one AC, which is in contrast with the 200 kHz map. In the combined map of MAC's the seabed from S1 and S2 are even more separated. The detailed analysis of the video footage with respect to the acoustic classification results per frequency indicates that, indeed, the AC's represent different seabed types. It is also shown that the AC's are able to distinguish between the soft sediments. However, the discrimination performance per frequency varies between the different sediment types. By combining the results of the different frequencies into a single map (Fig. 14d) the information gathered from each frequency are merged. Even though the combined map appears to be noisier, it indicates a more distinct discrimination of the seabed types.

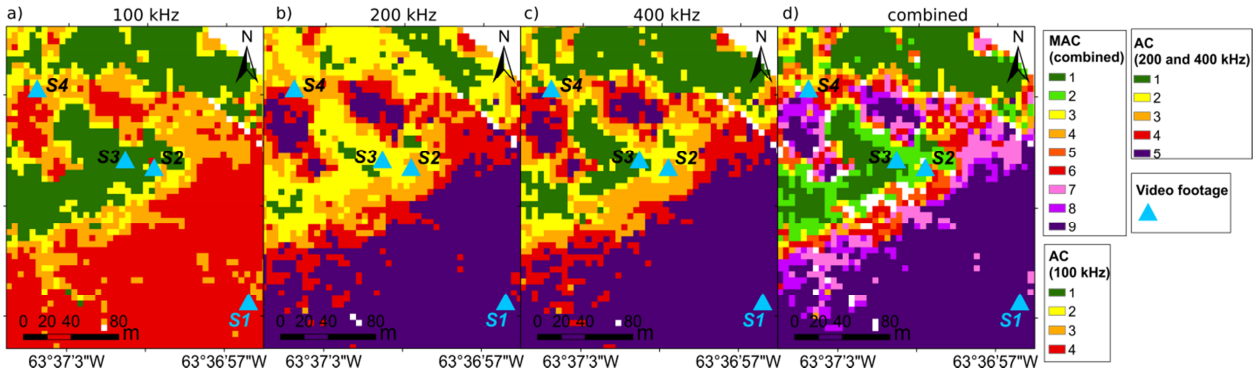

Fig. 14 Zoomed in area of the acoustic classification maps generated by the Bayesian method from a) 100 kHz, b) 200 kHz, c) 400 kHz and d) all frequencies. The area is indicated in Fig. 3 as area 3. The corresponding video footage to the samples S1 to S4 are displayed in Fig. 15.

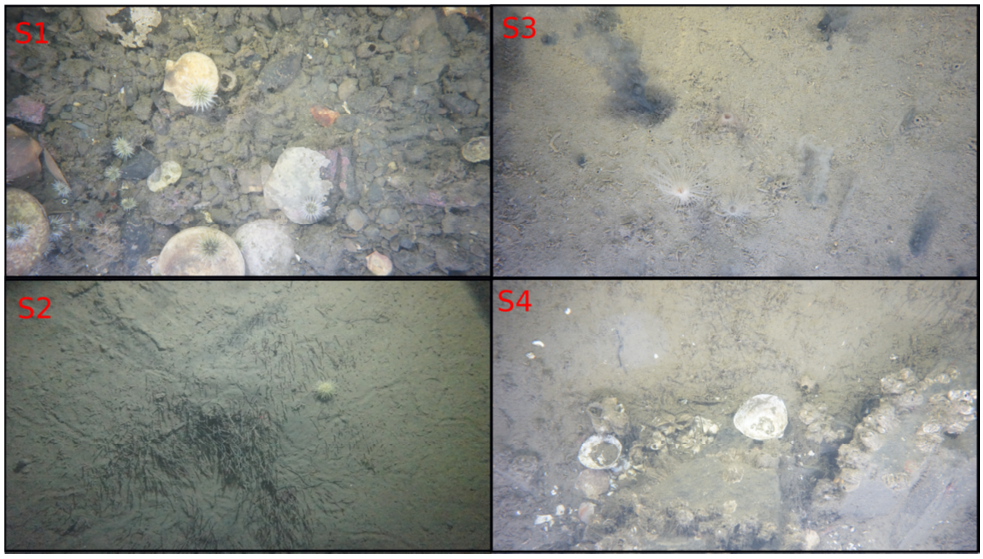

Fig. 15 Video footage of samples S1 to S4 indicated in Zoomed in area 3 of Fig 14.

5. Discussion

The Bayesian technique is applied to the processed MBES backscatter of the 100, 200 and 400 kHz datasets separately and the results are combined to a final multispectral acoustic classification map by accounting for the probability of misclassification. The main results with respect to the benefit of using several frequencies are threefold: 1) 200 and 400 kHz distinguish more acoustic classes than 100 kHz, 2) there is a benefit of using different frequencies for seabed classification with respect to the frequency and study area and 3) combining 100 and 400 kHz reveals the most additional information about the seabed. The first results are unexpected considering the backscatter mosaics indicating more spatial patterns at 100 kHz (Fig. 5a) (which was described in [11], but is also visible in the acoustic classification maps in Fig. 9). However, the analysis of the backscatter per incident angle, performed by the histogram fitting and the Chi-square test, indicates that more classes can be distinguished with increased frequency. Even though more spatial patterns are visible in the 100 kHz map they indicate similar backscatter signatures and shows up as the same acoustic classes. For instance, the circular structures, are hardly distinguishable from the seabed in the SW (consisting of a mixture of soft sediments and boulders) or NE (probably a large amount of benthic flora according to the video footage), whereas at 400 kHz these areas are clearly separated (Fig. 9). In the study of Hughes Clarke [10] where the MBES backscatter response of different frequencies (100, 200, 300 and 400 kHz) in

different sedimentological areas were investigated, more spatial pattern and a clearer distinction of the main facies at lower frequencies were observed. In addition, a high potential for higher frequencies (300 kHz) to divide the seabed types into further subclasses, which cannot be easily separated at 100 kHz, was observed in [10]. This is in correspondence with the first and third result presented in this paper (see above). Another observation, found in [10] but also indicated in a previous study [9], is that the frequency dependency is lower for rougher sediments and consequently the discrimination power gained by using different frequencies is larger for softer sediments. This is also observed in this study. The ARC's of the boulder/gravel sediments have very similar shapes whereas the ARC's of the soft sediments differ significantly (Fig. 3). The increased discrimination performance using different frequencies for smoother sediments is also shown in the acoustic class maps where the soft sediments are classified differently per frequency but the boulder/gravel sediments are represented consistently by the highest AC in each frequency (Fig. 9).

In this study, the results are mainly based on the analysis and interpretation of the acoustic backscatter signal considering an appropriate backscatter processing accounting for all sonar and environmental variables and a classification method accounting for the natural variability of the backscatter strength. Using the existing video footage only these results cannot clearly be verified. To investigate to what degree each AC and also each MAC represent different surficial or subsurface sediment characteristics, more video footage and especially physical samples (e.g., Box corer, Van Veen sampler or shallow cores) from the seabed and subsurface on predefined locations are needed. In particular, a grain size analysis is required to verify a correspondence of the lower AC's and MAC's with different sediment types. For instance, based on the video footage a discrimination between mud, silt, fine or medium sand is not possible. The verification of one of the most obvious improvements by using several frequencies in this study site, i.e. the clear distinction of the circular structures from the surrounding seabed in the combined MAC map (Fig. 12), would require ground truthing of the subsurface. According to Brown *et al.* [11] these structures represent dredge spoil features covered with mud. Due to the higher signal penetration of the lower frequencies (100 kHz), especially in very soft sediments, the backscatter is more influenced by the buried structures than by the actual seabed surface. This means that the acoustic maps of the different frequencies, and consequently the combined map, do not necessarily represent exactly the same part of the seabed with respect to depth. To what extent

different depths of the seabed contribute to the total backscatter strength can be described by the reflection coefficient and the absorption of sound in sediments. The reflection coefficient can be expressed as [18]

$$\mathrm{R}(\vartheta_{1)} = \frac{\rho_2 c_2 cos\vartheta_1 - \rho_1 c_1 cos\vartheta_2}{\rho_2 c_2 cos\vartheta_1 + \rho_1 c_1 cos\vartheta_2} \tag{13}$$

where $(\rho_1 c_1)$ and $(\rho_2 c_2)$ are the density and sound velocity of media 1 (water column) and media 2 (seabed). The incident angle is ϑ_1 (see Eq. 6) and the refracted angle is ϑ_2. The absorption coefficient in sediments α_S can be approximated with [27]

$$\alpha_S = 10\log(e^{\frac{-((\rho_2-1)2\pi f x)}{Dc}}) \tag{14}$$

where x is the distance in the sediment layer and D is a constant representing the internal structure of the sediment. Both equations show the influence of the sediment properties, density as well as frequency and incident angle on the penetration depth of the signal and consequently on the contribution of the volume backscattering to the total backscatter strength. The multispectral Bayesian technique accounts for the incident angle and frequency dependency while assigning relative backscatter values to acoustic classes. That comes along with the classification applied to incident angle and frequency separately which enables the multispectral Bayesian technique, theoretically, to retrieve acoustic classes representing different depths of the seabed. This is an advantage over classification techniques based on the backscatter mosaic where the angular information are removed by an angular response curve correction (e.g., [13], [28]).

6. Conclusions

In this study the Bayesian classification method is introduced for multispectral MBES backscatter. The classification method accounts for the natural variability of the backscatter strength by assuming the measured backscatter per beam and frequency to result from a number of discrete seafloor types that each correspond to a Gaussian distribution. Therefore, the multispectral Bayesian method employs the MBES backscatter per beam and frequency. In that regard, the acoustic classes are defined dependent on frequency and incident angle allowing for an evaluation and comparison among the acoustic classes obtained from different frequencies.

The acoustic classification results obtained from the different frequencies are combined to a so-called multispectral acoustic classification map by accounting for the probability of misclassification per frequency and acoustic class.

The multispectral Bayesian technique is applied to a multi-frequency (100, 200 and 400 kHz) backscatter dataset acquired with an R2Sonic 2026 MBES in the Bedford Basin, Canada in 2016. The systems allows to modify the operating frequency on a ping-by-ping basis. It is shown that the multispectral backscatter can be properly processed to be used for seabed classification. The main results with respect to the benefit of using several frequencies are threefold: 1) 200 and 400 kHz distinguish more acoustic classes than 100 kHz, 2) there is a benefit of using different frequencies for seabed classification with respect to the frequency and study area and 3) combining 100 and 400 kHz reveals the most additional information about the seabed. However, a quantification of the gained benefit from different frequencies using the existing video footage cannot clearly be accomplished for this study area. Additional video footage, physical grab samples from the seabed and subsurface would be required at predefined locations. Some correlation of the acoustic classes with the video footage could only be found for soft, mixed and hard substrata. A finer distinction is not feasible due to the complex seabed composition consisting of irregular distributed benthic flora and fauna and boulders as well as the presence of gas seeps. In addition, the grain sizes of the soft sediment is unknown hampering a finer classification as well. Still, a qualitative comparison to the video footage reveals a correlation of different seabed types to the acoustic classes and also an improved discrimination by combining 100, 200 and 400 kHz to a multispectral acoustic classification map. In essence, multispectral backscatter provides high potential to solve ambiguities in the relationship between single-frequency backscatter and certain sediment types.

The research of multispectral MBES backscatter is just in its initial implementation stage. The acoustic response of different sediment types for different frequencies has to be studied in more detail, which requires an extensive ground truthing. The use of even lower frequencies than 100 kHz appears to be promising for seabed classification. However, using low frequencies, it has to be investigated to what extent the backscatter strength represents the seabed or the very shallow subsurface due to the increased penetration of the signal. Finally, the establishment of reference areas for MBES backscatter calibration will provide promising opportunities to calibrate and secure an appropriate processing of multispectral backscatter.

References

[1] V. Lecours, M. F. J. Dolan, A. Micallef and V. L. Lucieer, "A review of marine geomorphometry, the quantitative study of the seafloor," *Hydrol. Earth Syst. Sci.,* vol. 20, no. 8, pp. 3207-3244, 2016.

[2] C. J. Brown, S. J. Smith, P. Lawton and J. T. Anderson, "Benthic habitat mapping: A review of progress towards improved understanding of the spatial ecology of the seafloor using acoustic techniques," *Estuarine, Coastal and Shelf Science,* vol. 92, pp. 50-520, 2011.

[3] K. L. Williams, D. R. Jackson, D. Tang, K. B. Briggs and E. I. Thorsos, "Acoustic backscattering from a sand and a sand/mud environment: Experiments and data/model comparison," *IEEE Journal of Oceanic Engineering,* vol. 34, no. 4, pp. 388-398, 2009.

[4] D. R. Jackson and M. D. Richardson, High-Frequency Seafloor Acoustics, New York: Springer Science, 2007.

[5] APL-UW, "High-Frequency Ocean Environmental Acoustic Models Handbook," Applied Physics Laboratory, University of Washington, Seattle, Washington, 1994.

[6] D. Buscombe, P. E. Grams and M. A. Kaplinski, "Compositional Signatures in Acoustic Backscatter Over Vegetated and Unvegetated Mixed Sand-Gravel Riverbeds," *Journal of Geophysical Research: Earth Surface,* vol. 122, pp. 1771-1793, 2017.

[7] H. Medwin and C. S. Clay, Fundamentals of Acoustical Oceanography (pp. 717), London: Academic Press., 1998.

[8] A. N. Ivakin and J. Sessarego, "High frequency broadband scattering from water-saturated granular sediments: Scaling effects," *Journal of Acoustical Society of America,* vol. 122, no. 5, 2007.

[9] R. J. Urick, "The backscattering of Sound from a Harbor Bottom," *Journal of the Acoustical Society of America,* vol. 26, no. 2, pp. 231-235, 1954.

[10] J. E. Hughes Clark, "Multispectral Acosutic Backscatter from Multibeam, Improved Classification Potential," National Harbor, Maryland, USA, 2015.

[11] C. J. Brown, J. Beaudoin, M. Brissette and V. Gazzola, "Setting the Stage for Multispectral Acoustic Backscatter Research," in *United States Hydrographic Conference 2017*, Galveston, Texas, USA, 2017.

[12] D. Lu and Q. Weng, "A survey of image classification methods and techniques for improving classification performance," *Int. Remote Sens.,* vol. 28, no. 5, pp. 823-870, 2007.

[13] M. Snellen, T. C. Gaida, L. Koop, E. Alevizos and D. G. Simons, "Performance of multibeam echosounder backscatter-based classification for monitoring sediment distributions using multitemporal large-scale ocean data sets," *IEEE Journal of Oceanic Engineering,* vol. 99, pp. 1-14, 2018.

[14] E. Alevizos, M. Snellen, D. G. Simons, K. Siemens and J. Greinert, “Acoustic discrimination of relatively homogeneous fine sediments using Bayesian classification on MBES data,” *Marine Geology,* vol. 370, pp. 31-42, 2015.

[15] D. G. Simons and M. Snellen, “A Bayesian approach to seafloor classification using multi-beam echo-sounder backscatter data,” *Applied Acoustics,* vol. 70, pp. 1258-1268, 2009.

[16] X. Lurton and G. Lamarche, “Backscatter measurements by seafloor-mapping sonars. Guidelines and Recommendations. 200p,” http://geohab.org/wp-content/uploads/2013/02/BWSG-REPORT-MAY2015.pdf, 2015.

[17] A. Amiri-Simkooei, M. Snellen and D. G. Simons, “Riverbed sediment classification using multi-beam echo-sounder backscatter data,” *Journal of Acoustical Society of America,* vol. 126, no. 4, pp. 1724-1738, 2009.

[18] X. Lurton, An Introduction to Underwater Acoustics, Heidelberg: Springer-Verlag, 2010.

[19] “www.seatronics-group.com,” 15 May 2014. [Online]. Available: https://seatronics-group.com/files/2714/1823/2979/R2_Sonic_2024_-_Manual.pdf. [Accessed 27 February 2018].

[20] R. E. Francois and G. R. Garrison, “Sound absorption based on ocean measurements. Part I: Pure water and magnesium sulfate contributions,” *Journal of the Acoustical Society of America,* vol. 72, pp. 896-907, 1982a.

[21] R. E. Francois and G. R. Garrison, “Sound absorption based on ocean measurements. Part II: Boric acid contribution and equation for total absorption,” *Journal of the Acoustical Society of America,* vol. 72, pp. 1879-1890, 1982b.

[22] A. N. Gavrilov, A. J. Duncan, R. D. McCauley, I. M. Parnum, J. D. Penrose and P. J. W. Siwabessy, “Characterization of the Seafloor in Australia’s Coastal Zone using acoustic techniques,” in *The International Conference 'Underwater Acoustic Measurements: Technologies and Results*, Crete, Greece, 2005.

[23] I. M. Parnum and A. N. Gavrilov, “High-frequency multibeam echo-sounder measurements of seafloor backscatter in shallow water: Part 2 - Mosaic production, analysis and classification,” *Underwater Technology,* vol. 30, no. 1, pp. 13-26, 2011.

[24] J. Collier and C. J. Brown, “Correlation of sidescan backscatter with grain size distribution of surficial seabed sediments,” *Marine Geology,* vol. 214, no. 4, pp. 431-449, 2005.

[25] I. Parnum and A. Gavrilov, “High-frequency seafloor acoustic backscatter from coastal marine habitats of Australia,” in *Proceedings of Acoustics*, Perth, Australia, 2012.

[26] L. Fonseca, L. Mayer, D. Orange and N. Driscoll, “The high-frequency backscattering angular response of gassy sediments: model/data comparison from Eel River Margin, California,” *Marine Geology,* vol. 209, pp. 131-145, 2004.

[27] D. D. Caulfield, Yim and Yung-Chang, “Prediction of shallow sub-bottom sediment acoustic impedance while estimating absorption and other looses,” *J. Canad. Soc. Explor. Geophys.,* 1983.

[28] C. J. Brown, B. J. Todd, E. K. Vladimir, V. E. Kostylev and R. A. Pickrill, “Image-based classification of multibeam sonar backscatter data for objective surficial sediment mapping of Georges Bank, Canada,” *Continental Shelf Research,* vol. 31, pp. 110-119, 2011.